A Comparison of CCM2–BATS Skin Temperature and Surface-Air Temperature with Satellite and Surface Observations

MENGLIN JIN, R. E. DICKINSON, AND A. M. VOGELMANN*

Institute of Atmospheric Physics, The University of Arizona, Tucson, Arizona

(Manuscript received 12 February 1996, in final form 19 July 1996)

ABSTRACT

This paper reports on two types of comparisons that were conducted. First, 10-yr modeled skin temperatures were compared with observations to evaluate model simulations of this quantity. The simulations were conducted with the NCAR CCM2 coupled with the Biosphere–Atmosphere Transfer Scheme (BATS). The observations were obtained from TIROS-N/HIRS-2 and the First ISLSCP Field Experiment in situ measurements. Second, modeled skin temperatures were compared with surface-air temperatures to illustrate the differences between them at various spatial and temporal resolutions. This is the first such study of skin temperature in a GCM.

When compared with the observations, it is evident that the CCM2–BATS can successfully reproduce many features of skin temperature, including its global-scale pattern, seasonal and diurnal variations, and the effects of the land surface type. However, modeled skin temperature seems to be underestimated in high latitudes in January and overestimated in low- and midlatitudes, especially over arid and semiarid regions in July.

Statistical analyses suggest that the differences between skin and surface-air temperatures are scale dependent. They differ the most at smaller scales and are most similar at larger scales (i.e., they differ the most for regional scales and diurnally, and agree more closely on monthly scales and hemispheric spatial scales). The similarity between skin and air temperatures averaged over monthly and large spatial scales implies that the well-established surface-air temperature measurements may be used to validate satellite-obtained skin temperatures. The differences between skin temperature and air temperature are greatest in the winter hemisphere. The monthly maximum skin temperature is greater than maximum air temperature by about 3.5°–5.5°C, and minimum skin temperature is less than minimum air temperature by 3.0°–4.5°C. For monthly time averaging and continental or hemispheric spatial scales, skin temperature is consistently lower than air temperature by about 0.5°–1.0°C.

This work also studies the effects of different land types, vegetative cover, soil wetness, and cloud cover on skin temperature. These effects are partially responsible for the differences between skin and surface-air temperatures. These results are similar to those from earlier studies done at specific sites.

1. Introduction

Surface temperature is an important climate variable, related to surface energy balance and the integrated thermal state of the atmosphere within the planetary boundary layer. The land surface is a complex system possessing many different elements, each having its own temperature and depending on different energy exchange processes. Traditionally, standard surface-air temperature measured by a sheltered thermometer 1.5–3.5 m above a flat grassy, well-ventilated surface has been referred to as surface temperature. Now with satellite technology, another surface temperature called skin temperature is becoming available globally (Susskind 1993).

Skin temperature, also referred to as radiometric temperature, is inferred from the thermal emission of the earth surface and is generally some average of the temperature of various canopy and soil surfaces. It is more directly related to surface properties than is the surface-air temperature, and hence is important for understanding many terrestrial biogeophysical processes. It is perhaps more physically meaningful and useful than surface-air temperature.

Although skin temperature is highly correlated with surface-air temperature, it differs in its diurnal, seasonal, and longer timescale variations. For some surfaces—for example, forests and deserts—skin temperature may differ significantly from the average air temperature over the surface. These differences are caused primarily by their different dependencies on land surface and atmospheric conditions, and can be used to infer information about the surface heat flux, vegetation properties, and soil moisture (Deardorff 1978; Sellers et al. 1992; Nemani et al. 1993; Dickinson 1989, 1994; Garratt 1995; Zeng and Dickinson

*Current affiliation: Center for Clouds, Chemistry and Climate, Scripps Institution of Oceanography, University of California, San Diego, La Jolla, California.

Corresponding author address: Menglin Jin, Institute of Atmospheric Physics, PAS Building 81, The University of Arizona, Tucson, AZ 85721.
E-mail: menglin@air.atmo.arizona.edu

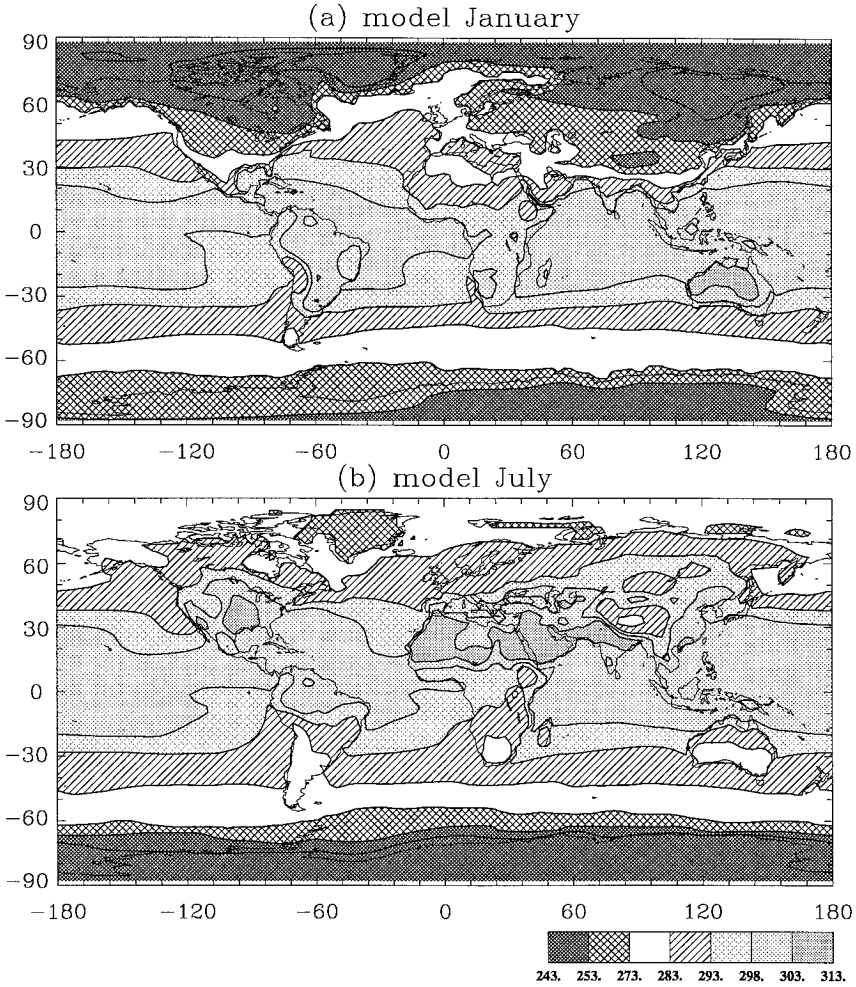

FIG. 1. The global distribution of skin temperature (T_{skin}) in Kelvins for January and July. (a) and (b) Model monthly averages; (c) and (d) from the 1979 satellite observations.

1997, manuscript submitted to *J. Climate*). For example, sensible heat fluxes are produced by a difference between instantaneous skin temperature and the overlying air temperature. This relationship has been used to estimate sensible heat fluxes from measured surface-air temperature and remotely derived skin temperature (Hall et al. 1992; Sun and Mahart 1995; Tselioudis et al. 1992; Vining and Blas 1992). Soil moisture, an important climate variable, might also be estimated remotely from skin temperature (Wang 1992). A number of algorithms are currently available for this purpose (Jackson et al. 1993; Mintz and Walker 1993; Sellers et al. 1990). They invert a model for the air–earth interface energy budget that contains skin temperature. By using such algorithms, Carlson et al. (1990) and Soden and Bretherton (1994) have quite successfully used remotely sensed data to produce maps of a moisture availability parameter. In the absence of external factors such as time of day, cloud cover and temperature advection, temporal and spatial variations in skin temperature depend primarily on variations in soil moisture, vegetation, and wind speed.

Before satellites, skin temperature could be measured only by ground-based radiometers or aircraft. Such observations are site specific and may fail to provide a convincing global or even regional view. Global measurements of skin temperature can be obtained from satellites that have been in place since the 1970s. Skin temperature has been derived from radiance measured by IR channel or microwave channel of satellite instruments. The former has been widely used but cannot get skin temperature under cloudy skies, while the latter has advantage of measuring surface radiance for clear and cloudy conditions. Skin temperature can be measured by thermal remote sensing instruments on geostationary satellites, such as GOES, METEOSAT, INSAT, and GMS, and polar-orbiting satellites, such as the AVHRR, HIRS-2, Landsat TM, and HCMM (Tran et al. 1992; Wetzel and Woodward 1987; Haskins et al. 1995; Soden and Bretherton 1994). For the IR channel method, there are two ways to retrieve skin temperature, either using detailed knowledge of the atmosphere profile and one IR channel obtained radiance (e.g., HIRS-2), or using two IR channels. To derive surface

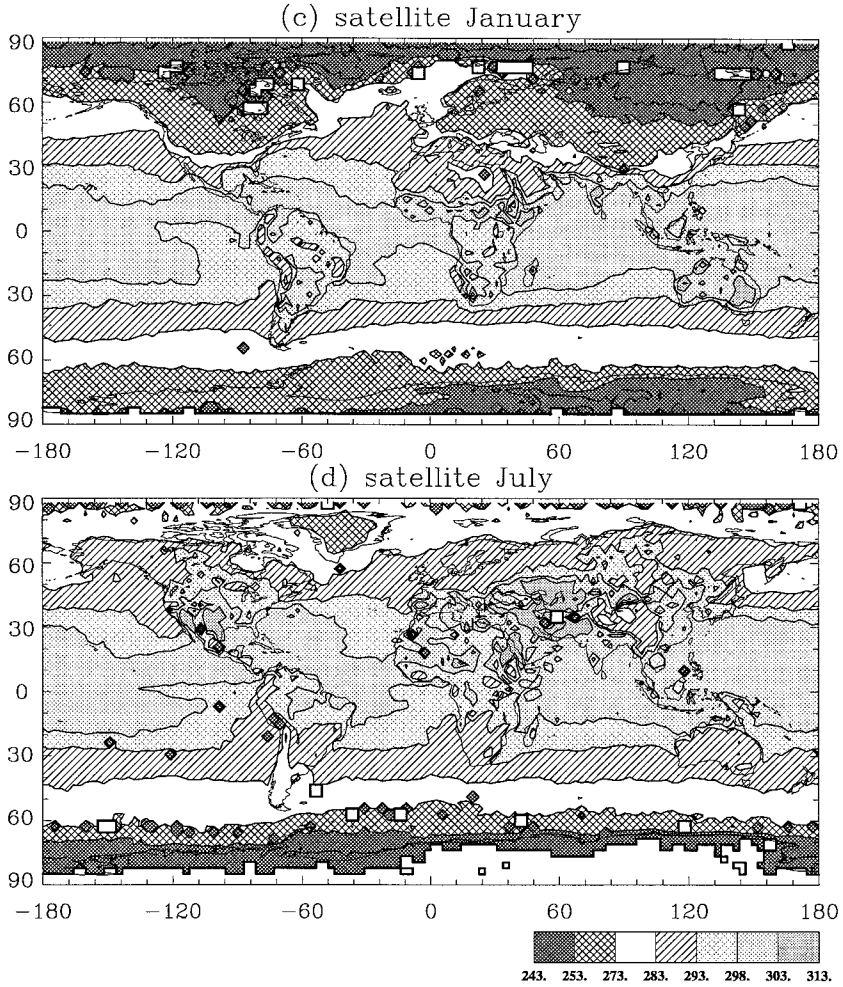

FIG. 1. (*Continued*)

temperature, both methods need to know the surface emissivity and water vapor content, because the radiance is a function of surface temperature, surface emissivity, and atmospheric conditions.

SST has been retrieved from satellites much earlier than land skin temperature. It is not a trivial step to apply the SST algorithm to land skin temperature because of the much more complicated properties of land surfaces and the dependence on overlying atmospheric conditions. At this time, adequate theoretical algorithms have been developed to derive skin temperature from satellites and their applications have been compared with the surface in situ data (Prata et al. 1995; Becker and Li 1995). The error of land skin temperature is about 1°–2°C, while the error of SST as little as 0.5°C.

Time series currently available from satellite-derived skin temperature are short compared to those for air temperature. These skin temperature data, however, have the potential advantages of better global coverage, higher resolution, and uniform quality. Hence, it is likely that they will become increasingly important. For comparisons with this new data source, the National Center for Atmospheric Research (NCAR) Community Climate Model version 2 (CCM2) with the Biosphere–Atmosphere Transfer Scheme (BATS) archives not only air temperature but also skin temperature. However, no attempt has been made previously to examine and verify the model-simulated skin temperatures. This work will assess the CCM2–BATS skin temperature simulations by comparing them with observations. This is the first such study of skin temperature in the context of a general circulation model (GCM).

The purpose of this work is to compare the CCM2–BATS skin temperature simulations with the current climate to address the following questions.

- Does the CCM2–BATS model provide realistic simulations of skin temperature?
- What are the geographical, seasonal, and diurnal features of skin temperature?
- What are the differences between skin temperature

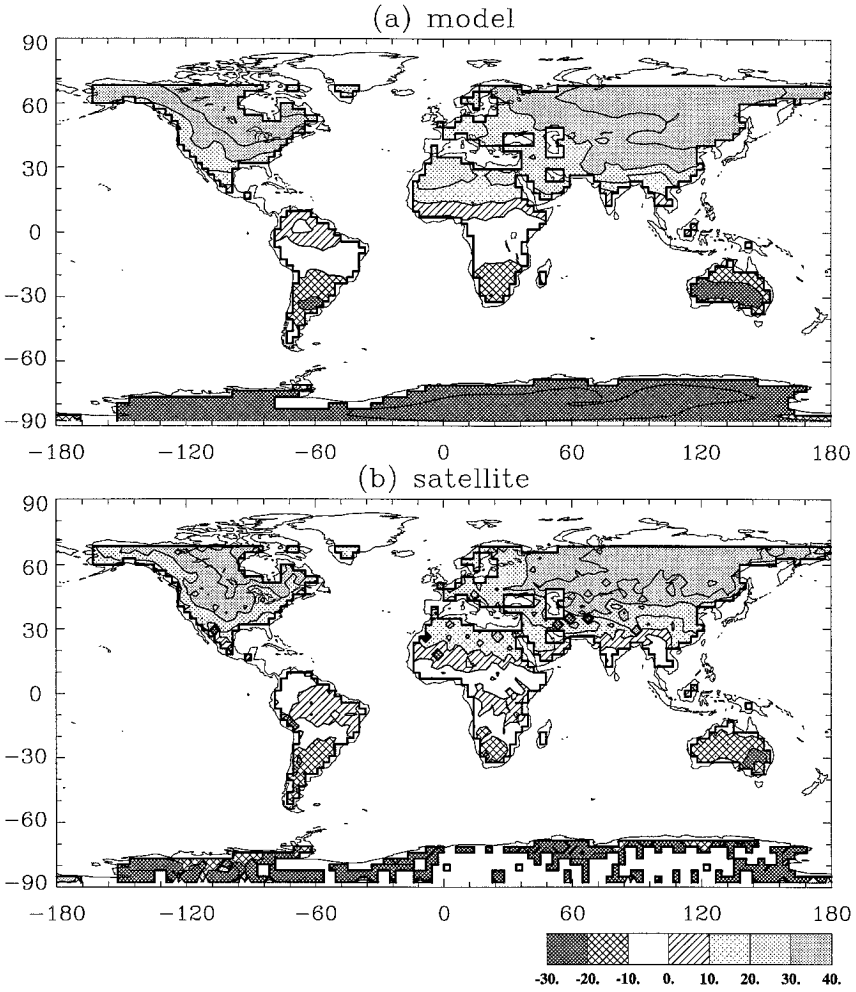

FIG. 2. The seasonal difference field of T_{skin} (July–January) in Kelvins. (a) Average of the 10-yr model simulation. (b) Satellite observations in 1979.

and surface-air temperature, and what factors determine these differences?

- How does vegetative cover influence skin temperature?

To address these questions, the general geographical and seasonal variations of the model-simulated skin temperature are compared to satellite-derived skin temperatures. The diurnal cycle of skin temperature and air temperature is studied at several sites using model hourly output from the climate model simulation and the First ISLSCP Field Experiment (FIFE) data. The studied sites were selected for their differences in vegetative cover and in latitudes. Because of the limited observations, some statistical analyses, involving correlation coefficients and empirical orthogonal function (EOF) analysis, were conducted with model data to prototype what can eventually be done with satellite data.

A detailed description of data is given in section 2. The results are presented in section 3, and the major conclusions are reviewed in the final section.

2. Data sources

Four temperature datasets are used: (a) surface-air temperature from the historical surface-based observations; (b) skin and surface-air temperatures from the FIFE observations; (c) skin temperature from satellite observations; and (d) skin and air temperatures modeled by CCM2–BATS.

a. Observed surface-air temperature

An observed, global, monthly, climatological, surface-air temperature dataset is employed (Halpert and Ropelewski 1992) to evaluate the model-air temperature simulations. This historical data was derived from 1200 station records, extending from the 1880s to the 1980s. It was provided by R. Jenne's group at NCAR and was remapped onto the GCM model grid with a resolution of approximately 2.8° lat × 2.8° long.

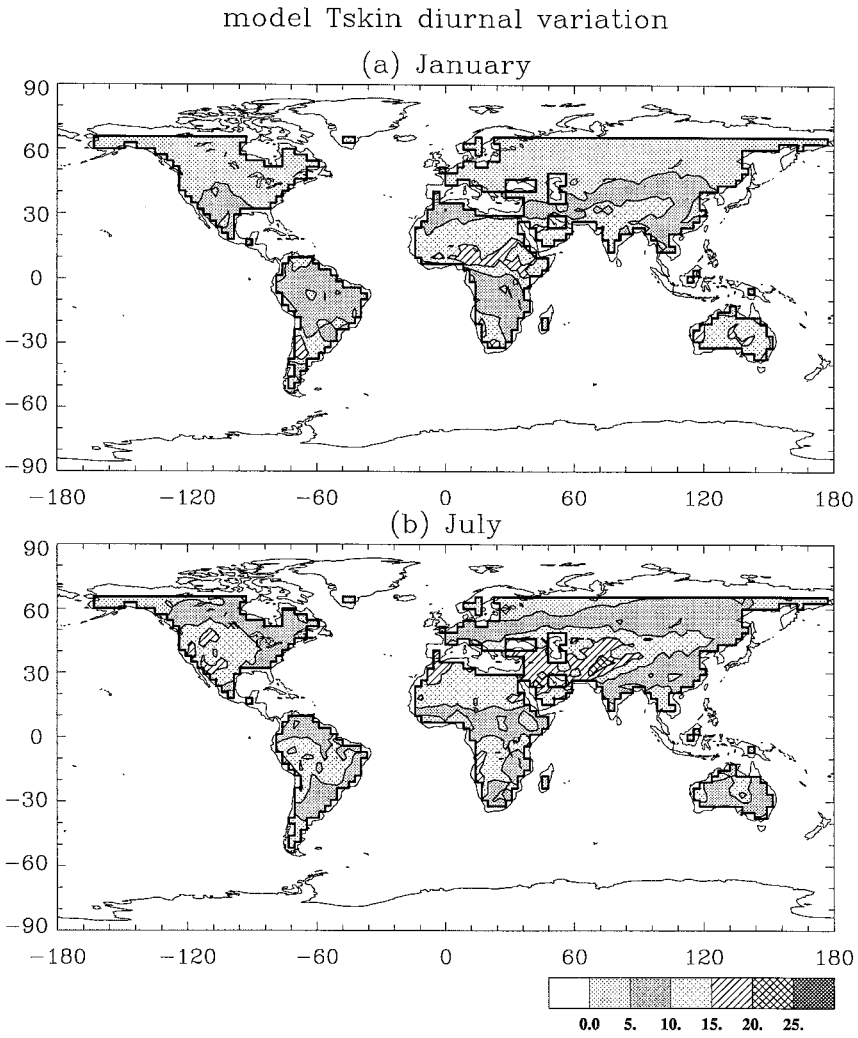

FIG. 3. Modeled diurnal variation of T_{skin}. Diurnal variation is the daytime skin temperature (T^{D}_{skin}) minus the nighttime skin temperature (T^{N}_{skin}) for (a) January and (b) July.

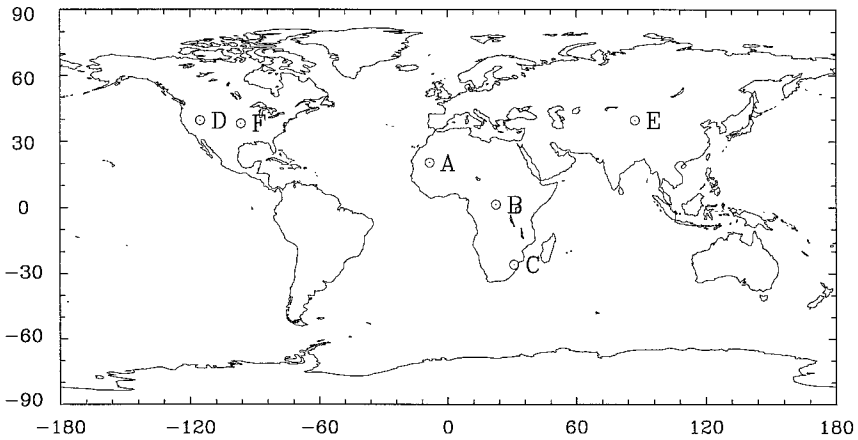

FIG. 4. Location of sites selected for the model diurnal cycle study: A (20.9°N, 8.4°W), desert; B (1.4°N, 22.5°E), evergreen broadleaf trees; C (26.5°S, 19.7°E), desert; D (40.5°N, 115.3°W), semidesert; E (40.5°N, 87.2°E), desert; and F (39.6°N, 96.4°W), short grass.

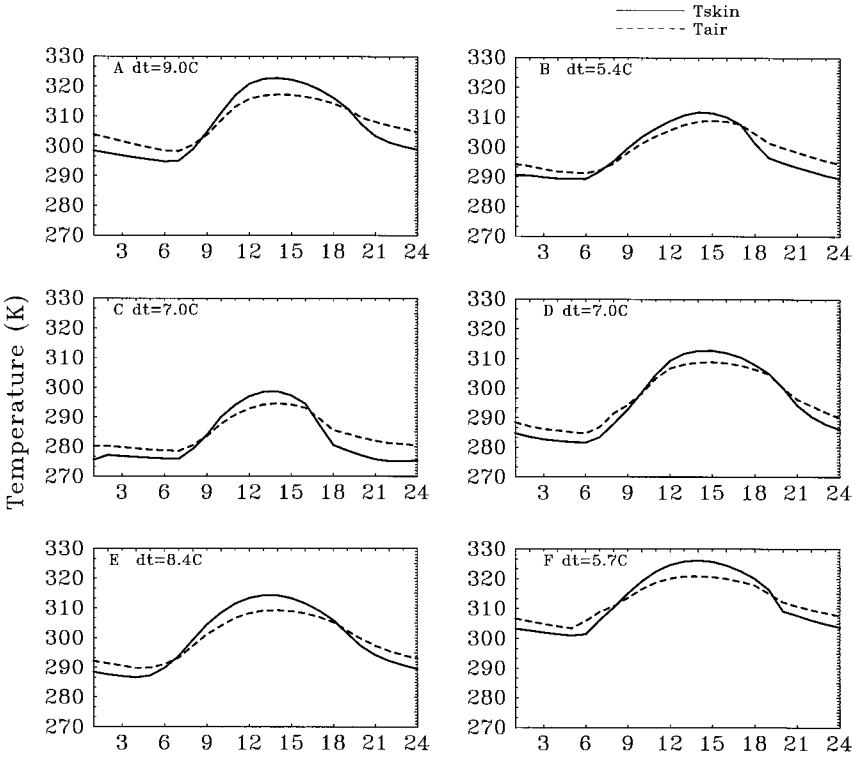

FIG. 5. Monthly mean diurnal cycle of the modeled T_{skin} and T_{air} for clear days in July. The x axis is the local time. The locations of the sites are given in Fig. 4. The differences between the diurnal range of T_{skin} and T_{air} are shown in the upper-left corner.

b. FIFE data

FIFE was an international, land–surface–atmosphere experiment where concentrated surface, airborne, and satellite measurements were made over a 15 km × 15 km test area near Manhattan, Kansas (about 39.05°N, 96.33°W). This experiment started in early 1987 and continued to 1989 (Sellers et al. 1992).

During FIFE, continuous data acquisition (satellite, automatic meteorological station, hydrological, and biometric data) occurred in two experimental phases in 1987 and 1989. Skin and surface-air temperatures were measured continuously at about 3 m above the surface by 22 Automated Meteorological Stations (AMS) distributed over the FIFE study area. These measurements were taken every 5 min and were block-averaged to half-hour intervals. Skin temperature was observed by IR thermometers, while surface-air temperature came from a measurement at 3 m. This work used site-averaged half-hourly data measured at FIFE July 1987.

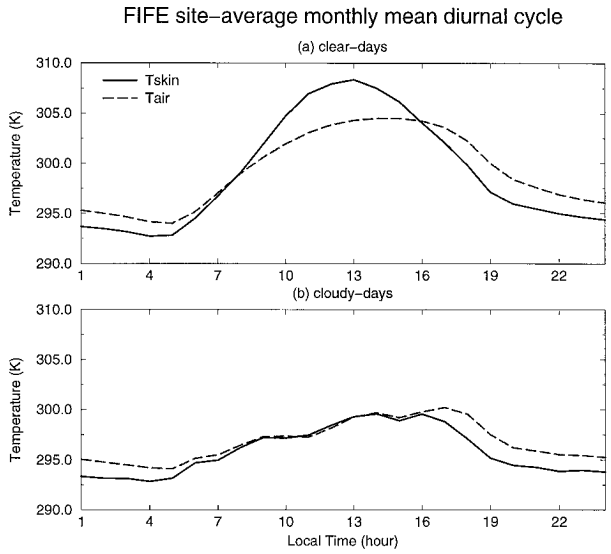

FIG. 6. Monthly mean diurnal cycle from FIFE observations. Measurements are obtained from all FIFE sites and averaged for July 1987 (a) clear days and (b) cloudy days.

c. Satellite-derived skin temperature

Satellite observations of skin temperature were retrieved from the High Resolution Infrared Radiation Sounder (HIRS-2) 4.3-μm band on TIROS-N Operational Vertical Sounder (TOVS) (Susskind et al. 1984). The retrievals were performed two times a day at a given location with local times of 0300 (referred to as nighttime) and 1500 (referred to as daytime) (Smith et al. 1979). The whole-day skin temperature (T_{skin}) is an average of the observed daytime skin temperature (T^D_{skin}) and nighttime skin temperature (T^N_{skin}).

HIRS-2 can retrieve atmospheric parameters, such as skin temperature, with as much as 80% cloud cover by using multiple fields of view. Any data with more than 80% cloudiness is flagged as too cloudy and not used. Also, the measurements of surface temperature are checked for internal consistency (closeness of fit with radiance residuals) and are rejected and not processed if they exceed a noise criterion.

Only atmospheric and sea surface temperatures have been validated against in situ data with any degree of confidence. Susskind (1993) reports a 2.2 K rms error for skin temperature. Currently, NOAA believes that with use of the NCEP product as a first guess, the retrieval error of atmospheric temperature is about 1.6 K. The accuracy of sea surface temperature is about 0.5 K. There are no reliable estimates for the accuracies of land-surface temperatures. Haskins et al. (1995) showed an accuracy of approximately 1–2 K for comparisons between seasonal differences and in situ data.

One year (1979) of TOVS-observed skin temperature data, including T_{skin}, T^{D}_{skin}, and T^{N}_{skin}, was provided by R. Haskins at the Jet Propulsion Laboratory (JPL). These data are currently available for December 1978 to November 1979 at a spatial resolution of 125 km $\times$ 125 km on a daily basis and are also remapped onto the 2.8° $\times$ 2.8° model grid.

d. Model-simulated data

Simulated skin and air temperatures were computed by the NCAR CCM2 coupled with BATS for 10 model years with hourly and monthly means archived. The model was run with a horizontal-spectral resolution of T42 (approximately a 2.8° $\times$ 2.8° transform grid) with 18 vertical levels.

The third generation of the NCAR CCM version 2.0 (CCM2), described in detail by Hack et al. (1993), was extensively redesigned and recoded from earlier versions of the CCM for ease of use and modification, and to improve the physical parameterizations, especially for surface temperature, surface energy exchanges, boundary layer transfers, moist convection, and cloud amount and its interaction with the radiation field. The changes to the model have resulted in a significantly improved simulation, particularly in the low latitudes (Hack et al. 1994).

The CCM2 is coupled with BATS (Dickinson et al. 1986, 1993), a detailed land model for interfacing with the CCM. BATS has three soil layers and one vegetative layer, nine prognostic variables, and 18 surface-cover types that are based on Olson et al. (1983), Matthews (1983, 1984), and Henderson-Sellers et al. (1986). BATS couples with the NCAR CCM through calculations of the transfers of momentum, sensible heat, and moisture between the earth's surface and atmospheric layers. Evaluations of the performance of the coupled model (BATS with CCM0, CCM1, and CCM2) for many simulated fields are available in Wilson et al. (1987a,b), Dickinson and Henderson-Sellers (1988), Henderson-Sellers (1990), Dickinson and Kennedy (1991), Henderson-Sellers et al. (1993), Bonan (1994), and Hahmann et al. (1995).

The CCM2–BATS simulations used here have revised cloud optical properties for the radiation parameterization that improves the radiation simulation, especially in the Northern Hemisphere at middle latitudes (Hahmann et al. 1995). The prescribed value of effective cloud droplet radius over land was changed from 10 to 5 μm and the distribution of the prescribed liquid water path was changed from a function of latitude to a function of the solar declination angle.

Skin temperature (T_{skin}) in BATS is the average of the soil and canopy effective radiative temperature as calculated from the following equation:

$$T^{4}_{\text{skin}} = \sigma_f T^{4}_{f} + (1 - \sigma_f) T^{4}_{g}, \tag{1}$$

where σ_f is the fractional vegetative cover, T_f is the leaf temperature, and T_g is the soil temperature. Over the ocean, the model T_{skin} is equal to the prescribed sea surface temperature (SST). In the CCM2–BATS output, T_{skin} represents an average of T^{D}_{skin} and T^{N}_{skin} weighted by the length of day and night, respectively, whereas T^{D}_{skin} and T^{N}_{skin} represent daytime and nighttime averages. Equation (1) is how the model currently estimates skin temperature, but it could be improved by model developers through the possible inclusion of additional boundary layer detail and realistic emissivity.

Air temperature (T_{air}) is calculated in the CCM2 and interpolated between the lowest model layer (about 70 m) and skin temperature using micrometerological theory for a short grass land type. Here, $T^{\max}_{\text{air}}$ and $T^{\min}_{\text{air}}$ are the modeled maximum and minimum surface-air temperatures. Modeled T_{air} here is determined from the average of $T^{\max}_{\text{air}}$ and $T^{\min}_{\text{air}}$, instead of the daily average value, to be consistent with the observed T_{air}.

3. Results

a. Skin temperature features

1) GLOBAL DISTRIBUTION

Figure 1 shows the global distribution of the 10-yr modeled skin temperatures and compares them with the 1979 satellite observations for January and July. The prescribed SST used by the model is evidently similar to the observed 1979 ocean skin temperature. Irregularities in the satellite-obtained skin temperature fields are caused by the HIRS retrieval with up to 80% cloud cover and compositing of these observations over the month, such that neighboring gridpoint values could have been observed days apart. The model results and satellite observations are qualitatively similar. Well-known features in the surface-air temperature climatology are clearly shared by the skin temperature. They both vary with latitude and season, and have a strong equator-to-pole temperature gradient with the highest values of temperature in the summer hemisphere, especially over extratropical continental regions. The coldest regions

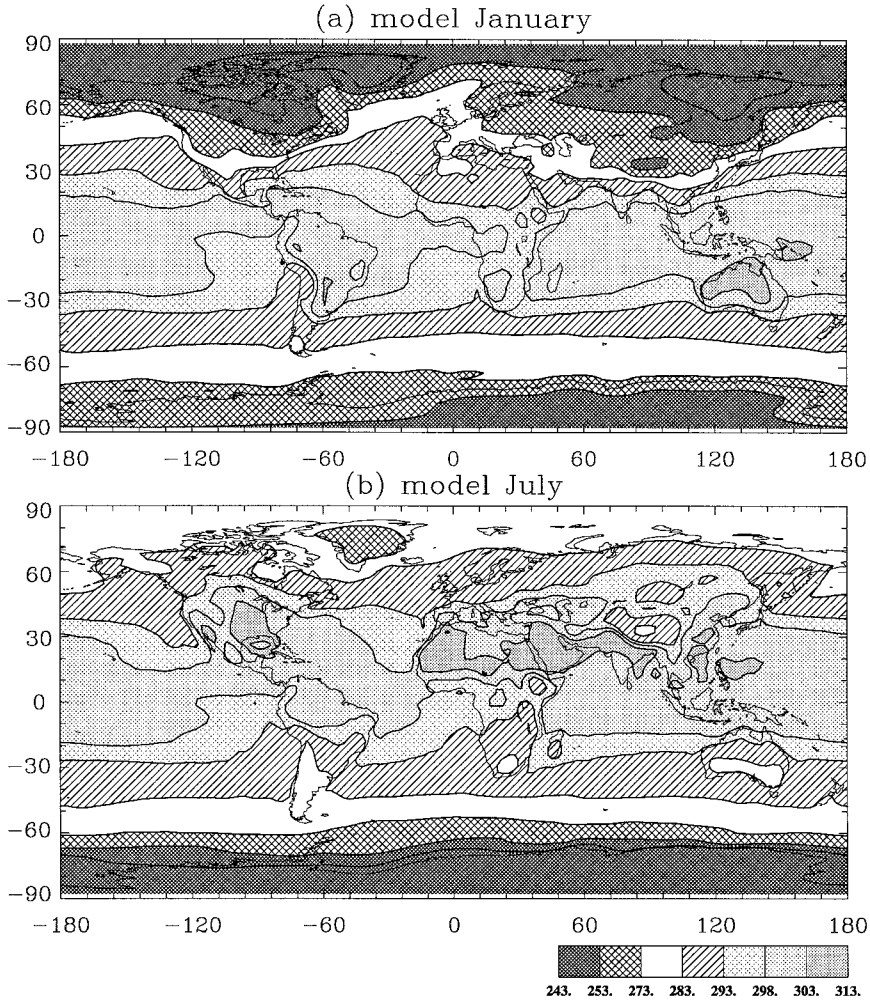

FIG. 7. Global distribution of monthly mean January and July T_{air}: (a) and (b) from the CCM simulation; (c) and (d) from standard surface observations.

are found over the northern parts of the continents in the Northern Hemisphere during winter (northeastern Siberia and Canada) and over Antarctica. In the Tropics, the meridional temperature gradients are small because of the small gradients in solar radiation and the large ocean fraction. The steepest horizontal temperature gradients are found in middle latitudes because of the influences of the gradient of solar insolation, the land-sea distribution, the type of land surface, and the surface topography. Land and ocean contrasts are notable.

Figure 2 compares differences of the July and January skin temperatures of the model output (Fig. 2a) with that from the 1979 satellite data (Fig. 2b). The Northern Hemisphere has a larger seasonal variation than the Southern Hemisphere because land covers 39% of the Northern Hemisphere but only 19% of the Southern Hemisphere. Maximum values occur in the centers of the large continents between 40° and 70°N.

Figures 1 and 2 show that model variables are very similar to observations, except that the model underestimates skin temperature in some high latitudes in winter by 1°–5°C, and overestimates it in summer at low and midlatitudes, especially over arid and semiarid areas where the discrepancies can be as much as 5°C. These disagreements are similar to those found from the calculated surface-air temperature fields. Hahmann et al. (1995) suggest that the cause for these discrepancies lies primarily in the overestimation of surface net radiation balance over these areas in summer. Other possible observational reasons for the disagreement are that the satellite has a polar orbit, which passes over a given point on the earth once each day and once each night, so the skin temperature is for a specific time and therefore should not be expected to agree exactly with the model values for the daytime and nighttime averages; and that errors occur in the satellite measurements.

2) DIURNAL CYCLE

The diurnal variation of skin temperature over land is an important climate process related to surface-air

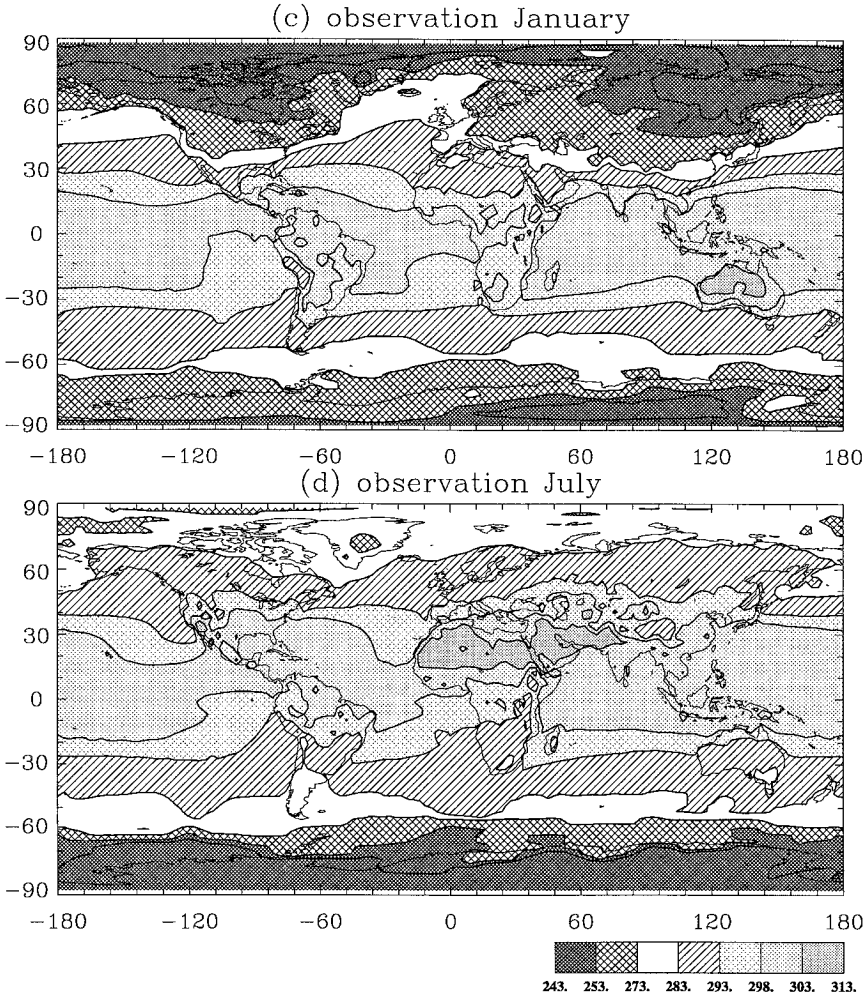

FIG. 7. (*Continued*)

temperature. How well it is simulated by a model is a good diagnostic of the model simulation of physical processes. Diurnal variations are especially sensitive to local conditions (including slope, ground wetness, snow cover, and vegetation) and to the state of atmosphere (including wind, humidity, and cloud cover).

Figure 3 is the skin temperature diurnal range (T^D_{skin}–T^N_{skin}) based on model simulations. It is obvious that the skin temperature generally has a larger diurnal variation in summer than it does in winter. The range exceeds 10°C in, particularly, southwestern Asia, southwestern United States and northern Mexico (July), subtropical South America, central Australia, and over the Sahara, a large strip centered at the Gobi (January).

Hourly output from the CCM2–BATS simulations for July was used to study the monthly diurnal variation of skin and surface-air temperatures. Figure 4 shows the six locations that were chosen to represent the different land cover types at different latitudes to illustrate the skin temperature and surface-air temperature diurnal cycle features. The locations and land surface types of these points are A (20.9°N, 8.4°W), desert; B (1.4°N, 22.5°E), evergreen broadleaf trees; C (26.5°S, 19.7°E), desert; D (40.5°N, 115.3°W), semidesert; E (40.5°N, 87.2°E), desert; and F (39.6°N, 96.4°W), short grass. Here A, C, and E are selected because they are over the same land cover type at different latitudes, while D, E, and F are different land cover types at the same latitude. For these model grids, hourly temperatures are averaged over all clear days in the month. Figure 5 shows the modeled diurnal cycles of skin and surface-air temperatures, whose general features will be compared with the observations (Fig. 6).

Figure 6 shows the monthly mean diurnal variation of skin and surface-air temperature from FIFE sites for clear (Fig. 6a) and cloudy (Fig. 6b) days, respectively. These data are obtained from FIFE measurements during July 1987. The 31 days are divided into clear and cloudy days according to the observed cloud amount, type, and height. Point F in Fig. 5 is the location of the FIFE site, therefore, we can compare the modeled and observed temperature features over F. Several conclusions are immediately apparent in Figs. 5 and 6. First, the patterns are very similar,

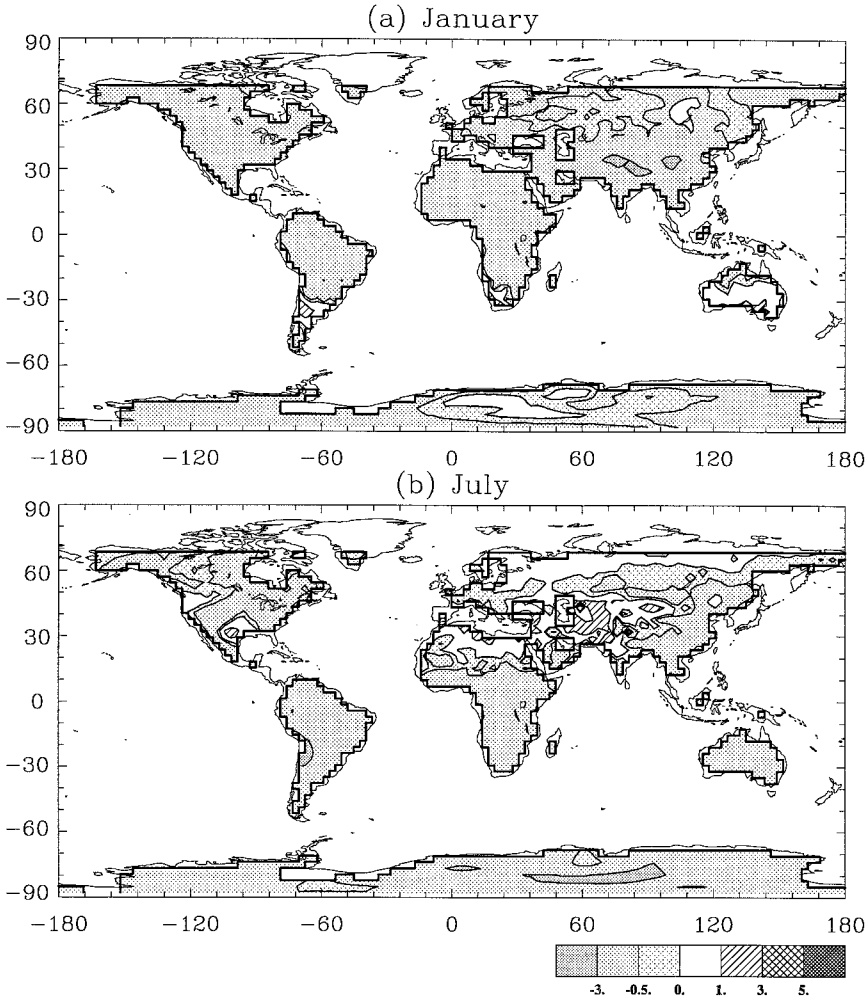

FIG. 8. Difference field between modeled skin and surface air temperatures ($T_{skin} - T_{air}$), based on 10-yr monthly mean simulations for (a) January and (b) July, respectively.

though the modeled skin temperature values in Fig. 5F are higher than the measured values in Fig. 6a for the short grass case. Second, air temperature has a smaller diurnal variation than does skin temperature, with its minimum higher and maximum lower than that of skin temperature. The disagreement between the simulation and measurement is consistent with the model's overestimation of net radiation, as pointed out earlier. Figure 6b further illustrates the influence of cloud cover on surface temperature. For a cloudy day, skin temperature has a smaller diurnal variation, and surface-air temperature is much closer to skin temperature than it is on a clear day. Although the midday skin temperatures are generally higher than surface-air temperatures, the day–night skin temperature (24-h average) is usually lower than the day–night surface-air temperature (the average of the maximum and minimum values). For example, the whole day average of T_{skin} clear day is 300.14 K, T_{air} is 300.81 K, and, for the cloudy days, T_{skin} is 300.10 K, and T_{air} is 300.15 K. Both the model simulations and FIFE observations show an average T_{skin} that is lower than T_{air}, as discussed later.

The differences between the diurnal range of modeled skin temperature and surface-air temperature are given in the top-left corner of each frame in Fig. 5. In all cases, the daily variations are obvious, with the peak temperatures near 1400–1500 LT, and the minimum at around sunrise. Over these land points, such variation is primarily due to the daytime warming of the surface by solar radiation. Different land types have different diurnal variations due to different surface characteristics, such as albedo, soil moisture, and vegetation type. For example, with the same solar forcing, case D, which is semidesert, has a larger diurnal amplitude than the short grass case F. In the low-latitude areas (cases A and C), the minimum skin temperatures occur in the early morning, after sunrise. The surface keeps cooling until sunrise, at which time solar radiation absorption begins to exceed longwave radiation loss. Diurnal variations are also dependent on the ampli-

tude of the solar forcing. Therefore, the diurnal variation of the summer hemisphere locations is larger than that of the winter hemisphere locations.

b. Differences between skin temperature and surface-air temperature

1) GLOBAL DISTRIBUTION

Because of the lack of skin temperature observations, we focus on model simulations to study the factors that influence the temperature over the diurnal cycle and the differences between skin and surface-air temperatures. The diurnal cycle of skin temperature is not only correlated with solar forcing, land cover, and vegetation type, but also with other factors such as convective activity, cloud coverage, and cloud type (Poetzsch-Heffter et al. 1995; Hendon and Woodberry 1993). The work shown in this section provides an example of what might be done with future satellite data to aid surface energy balance studies.

Figures 7c and 7d compare the observed climatology of surface-air temperature (described in section 2) with the surface-air temperature that is calculated from the model climatology for January and July (Figs. 7a and 7b). The simulations agree with the observations in terms of the distribution pattern, but in the Northern Hemisphere high latitudes, the model-simulated temperature is lower than the observations in winter and higher for most areas in summer (Hahmann et al. 1995). For example, the summertime simulated temperatures are 3.1°C higher averaged over North America and 0.6°C higher over Asia compared to the historical climatology.

Figure 8 compares the difference of the modeled monthly average skin temperature and surface-air temperature ($T_{skin} - T_{air}$) for January and July. Over the ocean, skin temperature is prescribed and does not change diurnally. Over some land areas in mid- to high latitudes, it is lower than surface-air temperature in winter but higher in summer. However, over much of North America and eastern Asia, simulated skin temperature is also lower than surface-air temperature in July, and likewise, in general, in low latitudes (10°N–20°S) for the whole year.

Figure 9 shows global and hemispheric averages of the calculated skin and surface-air temperatures over land as a function of month. Both temperatures have similar monthly variations. Skin temperature is consistently lower than surface-air temperature. In particular, global skin temperature is lower than surface-air temperature throughout the year by about 1.0°C. The differences are larger in the winter than in the summer hemisphere. Although monthly mean skin temperature is always lower than surface-air temperature, the sensible heat flux is generally from the surface to the atmosphere. This apparent contradiction comes from the nonlinear dependence of sensible heat fluxes on surface

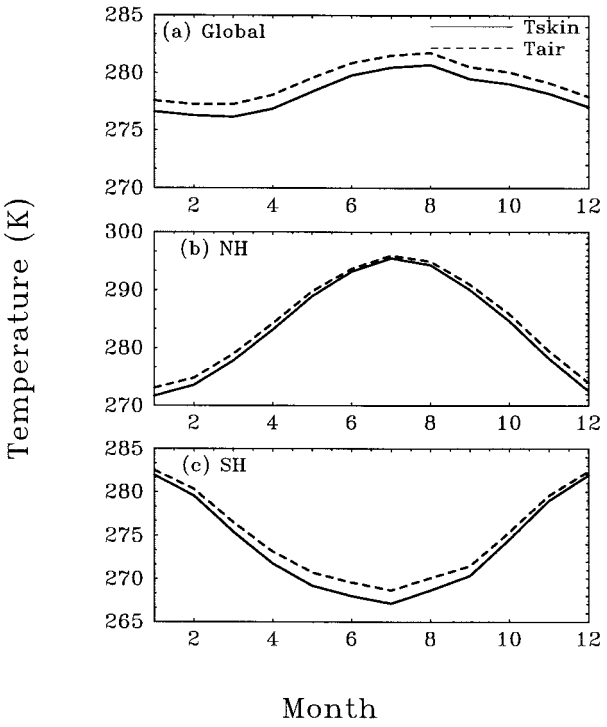

FIG. 9. The 10-yr modeled global and semihemispheric averages of the modeled T_{skin} and T_{air} over land as a function of month: (a) global, (b) Northern Hemisphere, and (c) Southern Hemisphere.

temperature differences. Sensible heat flux is proportional to the product of the vertical temperature differences and the heat transfer coefficient; the latter with the magnitude of the temperature drop from surface to air and thus has larger values at daytime than at nighttime (Smith et al. 1992).

To better understand the latitudinal contributions to the differences shown in Fig. 9, Fig. 10 shows the Northern Hemisphere monthly mean of skin temperature and surface-air temperature averaged over 20° latitudinal bands. Largest zonal variation is observed at midlatitudes, resulting from the effects of the large contrasts between the land and ocean on the temperature field. Although the skin temperature overall corresponds closely to surface-air temperature in a zonal average, it may behave differently at regional scales. For example, in January, skin temperature is higher than surface-air temperature over eastern Asia (~ 110°E, 20°–40°N) but lower than it over western Asia (~40°E).

Figures 5, 9, and 10, taken together, indicate that the differences between skin and surface-air temperatures depend on the temporal and spatial scales. Although skin temperature can significantly differ from surface-air temperature over a diurnal cycle or for regional scales, they are very similar for monthly time and hemispheric averages. Such scale-dependence corresponds to scales of the surface properties and processes, such as local soil moisture and vegetative cover. Thus, monthly or seasonal and continental or hemispheric averages might

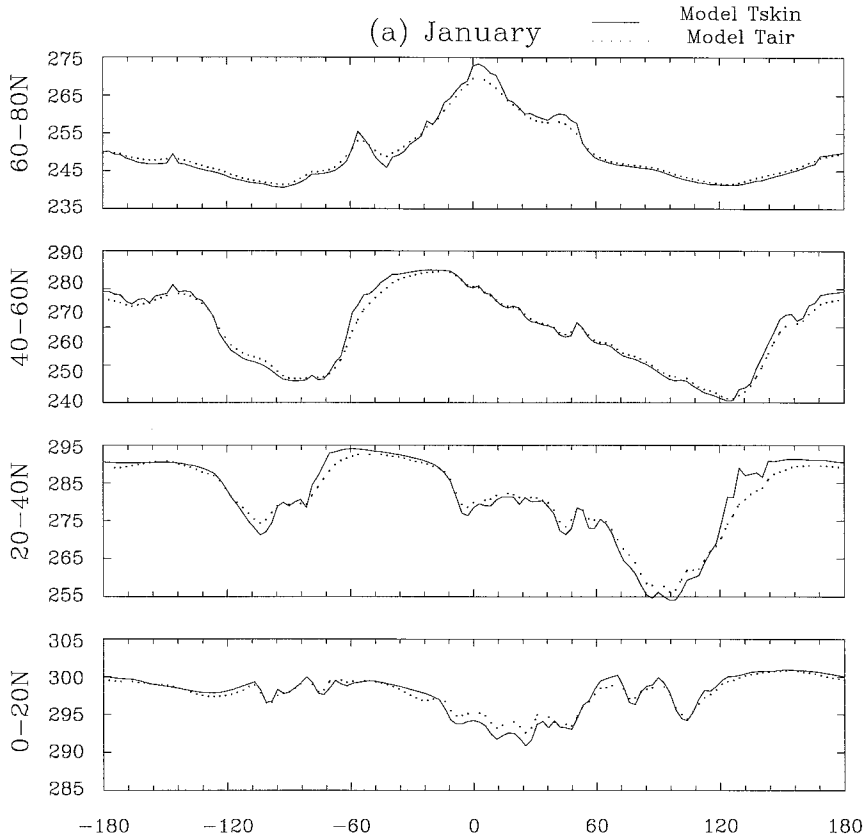

FIG. 10. Belt average of 10-yr modeled T_{skin} and T_{air} in (a) January and (b) July. Latitude bands are 0°–20°N, 20°–40°N, 40°–60°N, and 60°–80°N.

be the best to use to assess biases in satellite surface skin-temperature from surface-air temperature.

Figure 11 shows the correlation field between the model skin temperature and the surface-air temperature over land, based on 5 yr (model year 6–model year 10) of monthly mean simulations for January and July. The correlation coefficient r for a month is determined by

$$r = \frac{\text{cov}(T_{skin}, T_{air})}{S_{skin}S_{air}} \tag{2}$$

$$\text{cov}(T_{skin}, T_{air}) = \frac{1}{N-1}\sum_{i=1}^{N}[T_{skin}(i) - \bar{T}_{skin}] \times [T_{air}(i) - \bar{T}_{air}] \tag{3}$$

$$S_{skin} = \frac{1}{N-1}\sum_{i=1}^{N}[T_{skin}(i) - \bar{T}_{skin}]^2 \tag{4}$$

$$S_{air} = \frac{1}{N-1}\sum_{i=1}^{N}[T_{air}(i) - \bar{T}_{air}]^2, \tag{5}$$

where $\text{cov}(T_{skin}, T_{air})$ is covariance of T_{skin}, and T_{air}, S_{skin}, and S_{air} are standard deviations. Here, $N = 5$ for 5 model years, and $\bar{T}_{skin}$ and $\bar{T}_{air}$ are the monthly means for one grid cell. Figure 11 shows that skin temperature and surface-air temperature are highly positively correlated. Most areas have coefficients above 0.97. But relatively low values (0.70) are also found at low latitudes for the Northern Hemisphere for July.

To explain this feature, one model grid point (18.1°N, 19.7°E), with correlation coefficients of $r = 0.99$ in January and $r = 0.70$ in July, was chosen to illustrate the interannual variation (5-yr mean removed) of skin temperature, surface-air temperature, total cloud cover, and soil wetness (Fig. 12). It shows that skin temperature anomalies are less like the surface-air temperature anomalies in July than in January, and that, furthermore, July has larger variations in cloud cover and soil wetness. This suggests that differences between skin and surface-air temperature anomalies are associated with soil wetness and cloud amount, in addition to land type and vegetative cover.

The 10-yr model simulations were averaged over 30°–40°N desert areas. In these desert areas the vegetative cover should have minimal effects on the temperatures. Figure 13 presents the monthly variation of surface-layer soil wetness (SSW) and the differences between T_{skin} and T_{air} for this region. The temperature difference pattern is the reverse of that for the surface-layer soil moisture. The lowest SSW in summer is associated with highest T_{skin} relative to T_{air} at that time, T_{skin} close to T_{air},

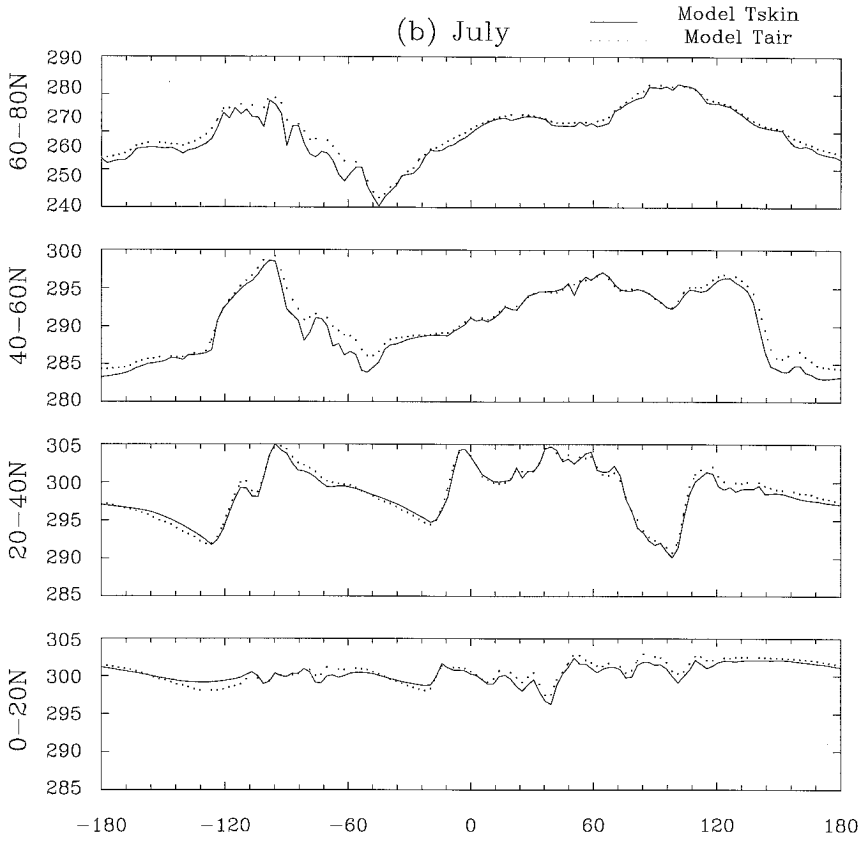

FIG. 10. (*Continued*)

as a result from larger daytime differences than at other time of year. With less soil moisture, hence less evaporation, there are larger sensible heat fluxes, and hence larger daytime differences. Likewise, the greater differences of the diurnal average in winter correspond to weaker daytime sensible fluxes because of the greater moisture fluxes and less solar radiation.

2) EOF ANALYSIS

The dominant modes of temperature are studied using an empirical orthogonal function (EOF) analysis of the skin temperature and the difference field between skin temperature and surface-air temperature. The EOF analysis represents the data by empirical functions that are obtained from interrelationships within the dataset and, since the EOFs are orthogonal, only a few are needed to efficiently represent the variance of the data fields. Their time series describe the evolution of the EOFs with time. The EOFs are ordered so that the first EOF explains the largest amount of the total variance of the original data. A thorough review of the formulation and properties of EOF analysis is given by Davis (1976) and a summary is provided by Trenberth and Paolino (1981). In brief, the EOFs are the eigenvectors of the covariance matrix obtained by the observations correlating in time at each grid point in space. Associated with each eigenvector is an eigenvalue that corresponds to the variance accounted for by the EOF. With this type of analysis, most of the variance of the temperature fields can usually be presented by only a few EOF patterns and their corresponding time series. EOF patterns are not predetermined but are found from interrelationships within the dataset. We have used the covariance matrix because we are interested in the actual anomalies (departures from the average) that occur.

The EOF analysis was performed on the multiyear collection of monthly mean model skin temperature. Graddock and Flood (1969) hypothesized that noise in the eigenvalues progresses geometrically, which would imply that temperature EOF components greater than three may not be significant. In this work, since only 10 yr of data are used, most attention is paid to the first eigenvector patterns (EOF1). EOF1, which explains the largest amount of the total variance, is given for skin temperature, in January and July, respectively. In Fig. 14, this mode explains 48.7% of the variance over the domain in January versus 26% for EOF2 (not shown). In July (Fig. 14b), EOF1 explains 49.9% of the variance. Similar patterns occur for the surface-air temperature fields (not shown). Globally, the strength of the departure is stronger in the winter than in summer.

This EOF1 (Fig. 14) pattern for January is similar to

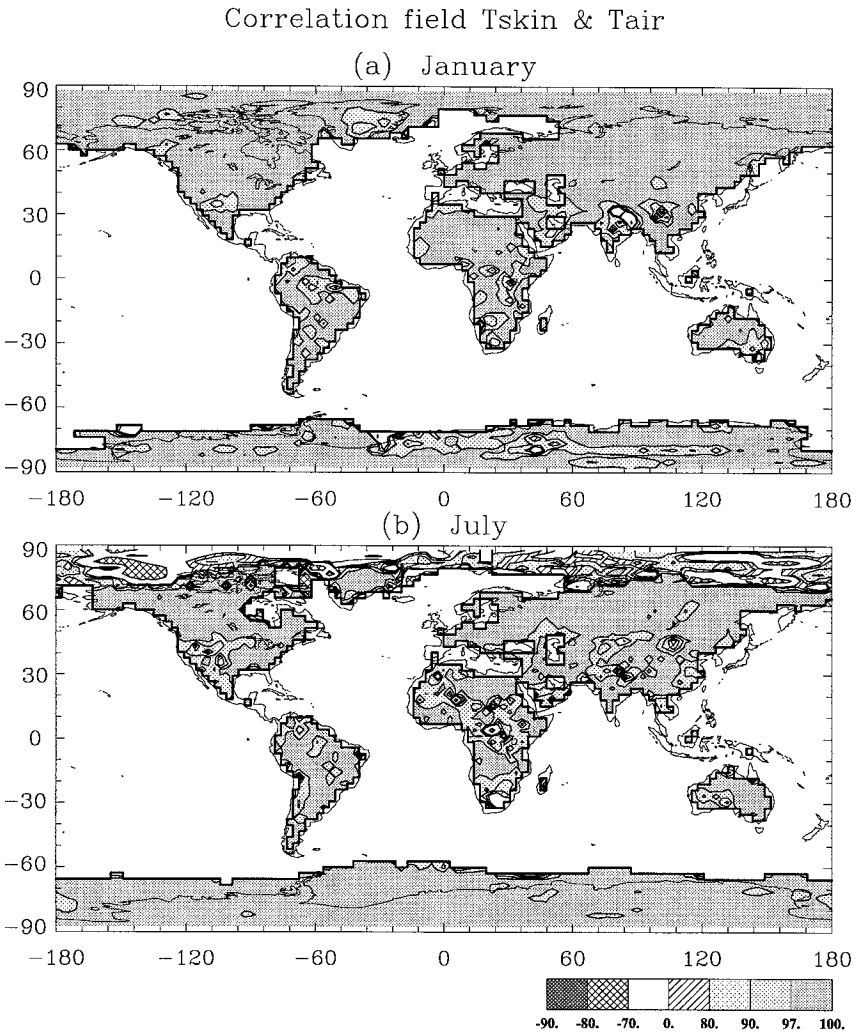

FIG. 11. The correlation coefficient field of the model skin and surface-air temperatures over land, based on the multiyear averages of simulations for (a) January and (b) July. The coefficients have been multiplied by 100.

the Atlantic seesaw pattern. The seesaw has been defined in terms of temperature anomalies between Greenland and Europe since 1840 (high temperatures on one side of the Atlantic, low on the other; Van Loon and Rogers 1978). There are two states of the seesaw: 1) Greenland below-normal temperatures (GB mode); and 2) Greenland above normal temperatures (GH mode). These two modes can be represented by opposite signs of the same EOF. The seesaw also was identified with the so-called North Atlantic oscillation (NAO), originally defined by Walker and Bliss (1932). The NAO is a teleconnection pattern with centers of action of opposing sign in the regions of the Icelandic low and the Azore high. Both Kutzbatch (1970) and Kidson (1975) related their EOF1 pattern for January analysis to the NAO. Wallace and Gutzler (1981) found a similar result and suggest that EOF1 for winter should not be viewed as having a one-to-one correspondence with the NAO.

Figure 15 is the first eigenvector pattern for skin temperature and surface-air temperature difference fields in January and July. It suggests a latitudinal wavelike oscillation pattern on the global scale. The differences in January and July are obvious, especially over subtropical desert areas. For example in January, the Sahara has large positive values and Australia has negative values, but in July the opposite is observed over these areas. Similar changes also occur in the southeastern United States. Variations of temperature differences with land cover apparently explain much of the pattern seen in Fig. 15.

c. Daytime and nighttime temperatures

Previous figures (Figs. 5 and 6) showed the diurnal behavior of temperatures. We now consider daytime and nighttime temperatures separately to illustrate their relative contributions to the whole-day temperature, and to

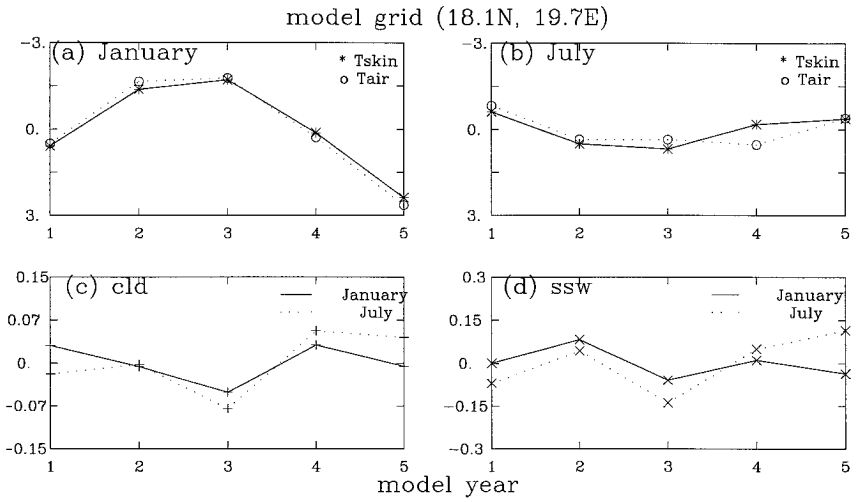

FIG. 12. Interannual anomalies of T_{skin}, T_{air}, cloud fraction, and soil wetness for a model grid (18.1°N, 19.7°E). (a), (b) The T_{skin} and T_{air} in January and July, respectively; (c) the total cloud cover fraction (cld) in January and July; and (d) the surface-layer soil wetness (SSW) in mm for January and July.

the possible dependencies of the differences between skin and surface-air temperatures on various land covers.

Figure 16 illustrates the definitions of various temperature concepts used in this work for a diurnal cycle at a model grid point. Here, T_{skin} stored in the model output is defined as the average of T^D_{skin} (daytime average) and T^N_{skin} (nighttime average), while T_{air} is $0.5 \times (T^{max}_{air} + T^{min}_{air})$. Here, T^{max}_{skin} and T^{min}_{skin} are maximum and minimum T_{skin}, respectively.

In Fig. 16, instantaneous skin temperature is generally higher than air temperature in the daytime and lower at night, consistent with the diurnal radiative forcing. Here, T^D_{skin} is somewhat less than T^{max}_{air}, and T^N_{skin} is somewhat greater than T^{min}_{air}. Typically, $T^D_{skin} - T^N_{skin}$ is almost 60% of the full day–night range of T_{skin}. For example, typical ranges are 25°C for minimum to maximum T_{skin}, 20°C for T^{max}_{air} to T^{min}_{air}, and 15°C for $T^D_{skin} - T^N_{skin}$. Therefore, the day–night average of T_{skin} and T_{air} typically differ by

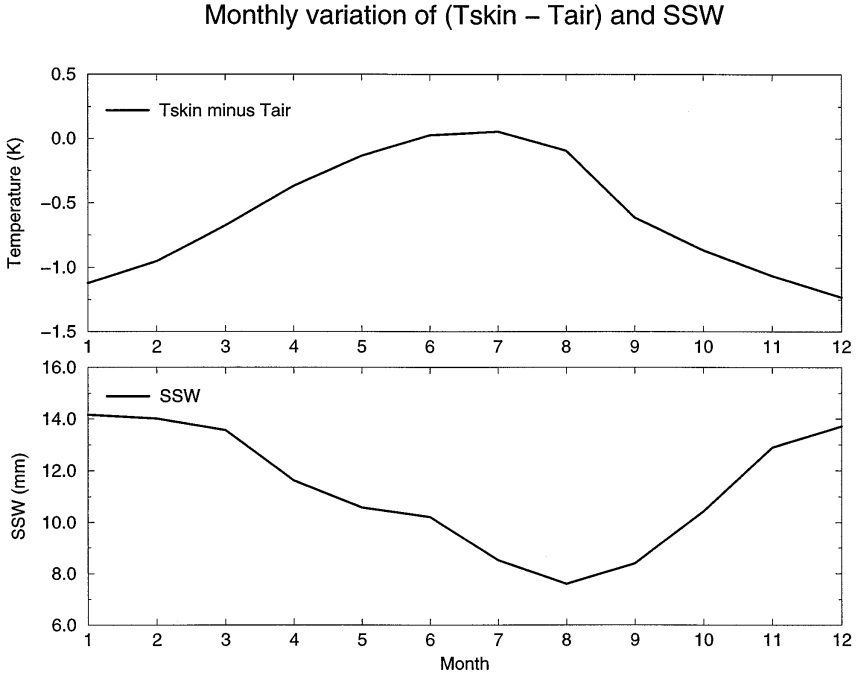

FIG. 13. The monthly variation of surface-layer soil moisture and of the difference between T_{skin} and T_{air}. Data are obtained from 10-yr model simulation, averaged over 30°–40°N desert areas.

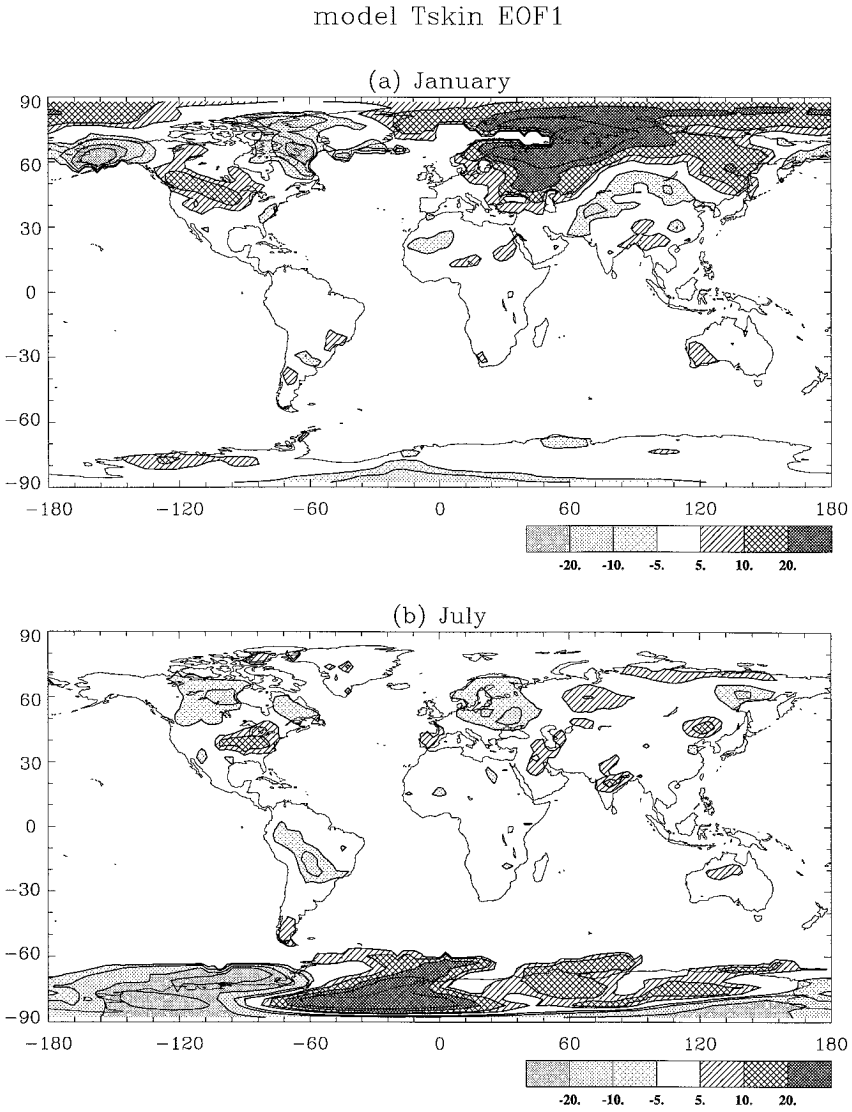

FIG. 14. First eigenvector for the 10-yr simulated T_{skin}: (a) January, (b) July.

1°–2°C with T_{skin} being slightly colder. Consequently, we expect T^D_{skin} to be less by up to several degrees than T^{max}_{air} and T^N_{skin} to exceed T^{min}_{air} by up to several degrees. To simplify the discussion in the following analysis, we have approximately converted T^D_{skin} to T^{max}_{skin} and T^N_{skin} to T^{min}_{skin} by adding 7.43°C to T^D_{skin} and subtracting 4.51°C to T^N_{skin}, using the values given in Fig. 16. We could expect, in reality, that these factors would vary between cover types according to the amplitude of the diurnal cycle for that cover.

To study the influences of land type on daytime and nighttime temperature Fig. 17 shows the monthly mean differences between maximum and minimum skin temperatures (T^{max}_{skin}, T^{min}_{skin}) and T^{max}_{air}, T^{min}_{air}. These two pairs ($T^{max}_{skin} - T^{max}_{air}$; $T^{min}_{skin} - T^{min}_{air}$) are studied for four different vegetation types: crop/mixed farming, evergreen shrub, deciduous broadleaf tree, and desert. Model data from the 10-yr simulation are averaged over 30°–40°N. It should be recalled that the air temperatures over all surfaces were related to that of the lowest model level assuming roughness of a shortgrass, so that the effects of differences due to the height of vegetation have largely been removed.

Figure 17 shows that all land covers have daytime air temperatures less coupled to skin in late summer and fall than in winter and spring. The deciduous broadleaf tree and evergreen shrub covers appear to have the least daytime coupling between skin and air temperatures, and the crop also has this distinction for almost all close-to-summer months at night. The deserts show the least seasonal variation, both day and night, and the smallest departure of air from skin temperature. The crop and broadleaf covers show a noticeable seasonal pattern in their nighttime temperature difference, with summer air

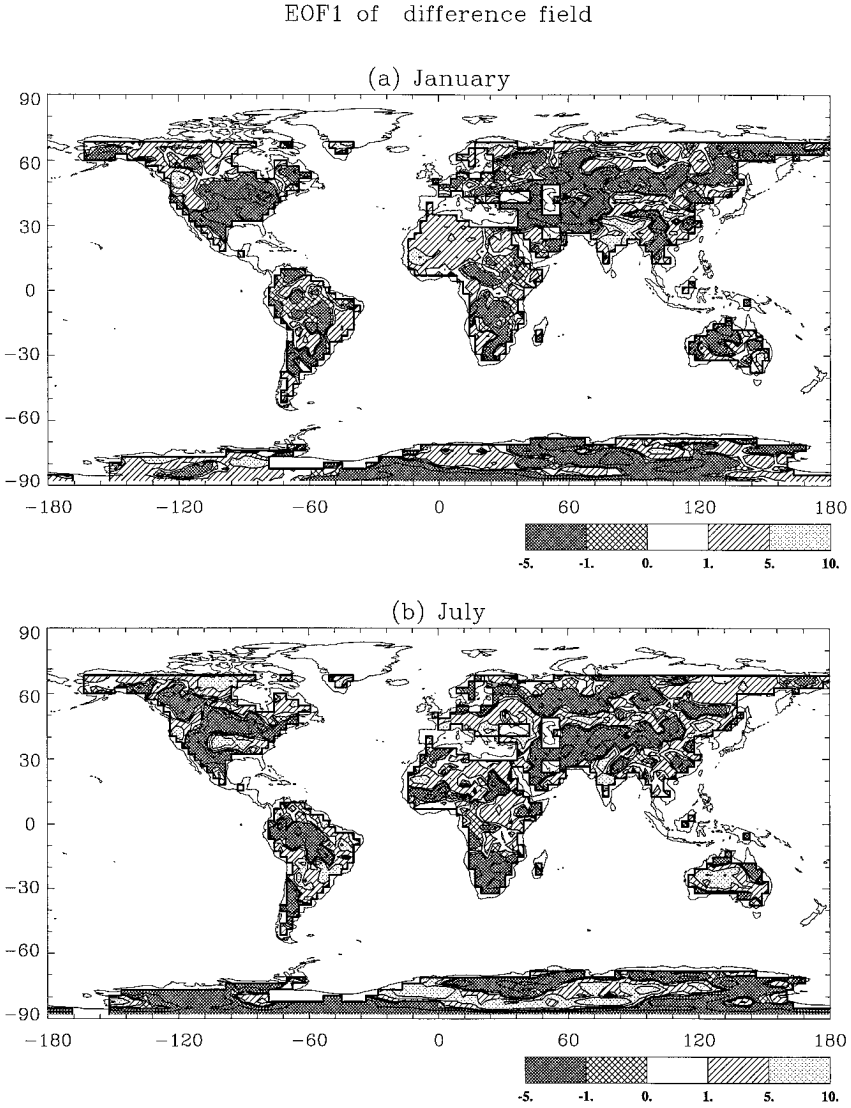

FIG. 15. First eigenvector for the difference field of the modeled T_{skin} and T_{air} (T_{skin} minus T_{air}): (a) January, (b) July.

temperatures farthest from skin temperature. Some of these relative results may be counter to what would be expected from the micrometeorology of these sites and may be an artifact of the normalization of air temperatures to a short grass roughness and to the use of the constant factors from Fig. 16 to infer the maximum and minimum skin temperatures.

Generally, in each month of the whole year, T_{skin}^{max} is greater than T_{air}^{max} by about 3.5°–5.5°C, and T_{skin}^{min} is less than T_{air}^{min} by about 3.0°–4.5°C. In summer, air temperature is farther from skin both in daytime and nighttime than in winter. The larger-positive daytime values in summer are compensated for by the larger-negative nighttime values, and result in less differences between skin and air temperatures in summer than in winter, as presented earlier.

Different vegetation covers have different temperatures that vary seasonally. These differences are controlled by the differences in surface roughness and albedo; by the variations in incident solar radiation, depending on its seasonality and reflection by cloud cover; by the differences in precipitation, hence evapotranspiration, and possibly other differences in surface meteorology.

4. Conclusions

This paper examines model skin temperature simulations over land, and differences between skin and air temperature at various temporal and spatial scales. We conclude that the model-simulated skin temperature is adequate for further use in studying skin temperature. The differences between the two kinds of surface temperatures are associated with vegetative cover/land type,

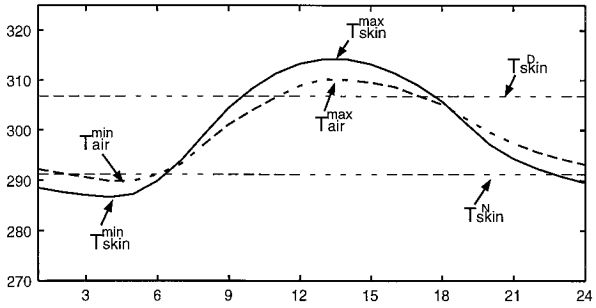

T_{skin}

	T_{skin}^{max}	T_{skin}^{min}	T_{skin}^{D}	T_{skin}^{N}	$T_{skin} = \frac{\text{dayhour} * T_{skin}^{D} + \text{nighthour} * T_{skin}^{N}}{24}$
Temperature (K)	314.25	286.65	306.82	291.16	299.75

T_{air}

	T_{air}^{max}	T_{air}^{min}	$T_{air} = \frac{T_{air}^{max} + T_{air}^{min}}{2}$
Temperature (K)	310.22	289.86	300.04

FIG. 16. Values and positions of different temperatures in one typical model day of July. T_{skin}^{max} is the maximum T_{skin}, and T_{skin}^{min} is the minimum T_{skin}. T_{skin}^{D} is the daytime skin temperature, and T_{skin}^{N} is the nighttime skin temperature. T_{air}^{max} and T_{air}^{min} are the maximum and minimum values of surface-air temperature, respectively. The tables give the values for each of these temperatures. T_{skin} is the hour-weighted average of T_{skin}^{D} and T_{skin}^{N}. T_{air} is the average of T_{air}^{max} and T_{air}^{min}.

soil moisture, and cloud conditions. It is gratifying that these results are consistent with past micrometeorological studies (Huband and Monteith 1986; Crosson et al. 1993), but their extension to large scales is not self-evident, and so this is one of the emphasized results of the present study.

The CCM2–BATS reasonably reproduces the measured features of skin temperature, including its global-scale pattern, seasonal and diurnal variation, and the effects of land surface and vegetative cover. However, some discrepancies between model simulations and observations are identified. Compared with 1979 satellite observations, the model underestimates skin temperature in January in some areas and overestimates it in July in low and midlatitudes, especially over arid and semiarid regions where the difference can be as much as 5°C. These disagreements are partially the result of the unrealistic simulation of the surface net radiation balance and the fact that the model data is a climatological average for clear and cloudy skies, whereas the satellite data is for one particular year of clear-sky conditions.

It is evident that skin temperature has many features that are similar to those of surface-air temperature. In particular, when focusing on monthly timescales and hemispheric spatial scales, surface-air temperature corresponds closely to skin temperature, so that ground-observed surface-air temperature may be used to check the relative accuracy of the patterns of satellite-observed skin temperature.

Skin temperature has an obvious equator-to-pole distribution and varies with latitude and season. The Northern Hemisphere, with its greater continentality, has larger seasonal and diurnal variations of skin temperature than does the Southern Hemisphere. EOF analyses show that, in January, the EOF1 of skin temperature is consistent with the Atlantic seesaw, Greenland below-normal (GB) mode, which is originally found in the surface-air temperature field.

The differences between skin and surface-air temperatures are scale-dependent and depend strongly on the diurnal cycle. Daytime skin temperature is somewhat greater than surface-air temperature, and nighttime skin temperature generally is lower than air temperature. The monthly averaged maximum skin temperature is greater than maximum air temperature by about 3.5°–5.5°C, and minimum skin temperature is less than minimum air temperature by 3.0°–4.5°C. These values will vary with season and latitudes. For the monthly time and conti-

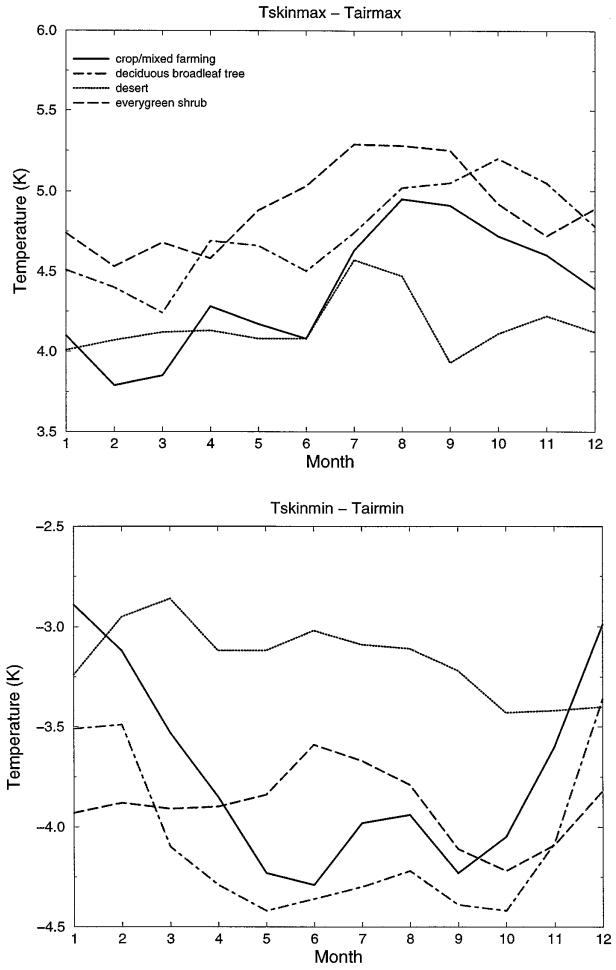

FIG. 17. Monthly mean differences between (a) T_{skin}^{max}, T_{air}^{max} and (b) T_{skin}^{min}, T_{air}^{min} for four kinds of vegetative cover. Data is obtained from 10-yr model simulation. In the plot, $T_{skinmax}$, $T_{skinmin}$ stand for T_{skin}^{max}, T_{skin}^{min}, and T_{max}, T_{min} stand for T_{air}^{max}, T_{air}^{min}, respectively.

nental or hemispheric spatial scales, skin temperature is constantly lower than air temperature by 0.5°–1.0°C.

Because the differences between skin and air temperatures are important for interpreting the surface energy, the factors that influence these differences are emphasized in this paper. We have shown the cloud amount has a significant influence on the two temperatures and their differences (Fig. 6). Solar radiation (represented by the latitude here) and vegetation type have obvious effect on the skin and air temperatures (Fig. 5). Figure 13 shows that T_{skin} and T_{air} are closely related to the variation of soil moisture, which implies that soil moisture plays an important role in the surface temperature differences. The relationships between skin and air temperatures are very complicated and link with many other physical processes in coupling between the surface and atmosphere.

This work has used only 1 yr of satellite-observed skin temperature. Because of this data limitation, we have relied on model simulations to analyze the relationships between skin and surface-air temperatures. More extensive skin temperature observations would be required to evaluate the relationships that we found.

Acknowledgments. We thank Robert Haskins of Jet Propulsion Laboratories for providing satellite data and helpful discussions. Thanks to Cas Sprout for help in editing and to two anonymous reviewers for their review comments. We will also like to thank Andrea Hahmann for revision comments on various drafts. This work was supported by NASA EOS Interdisciplinary Scientific Research Program (U.P.N. 429-82-22; U.P.N. 428-81-22).

REFERENCES

Becker, F., and Z. Li, 1995: Surface temperature and emissivity at various scales: Definition, measurement and related problems. *Remote Sens. Rev.,* **12,** 225–253.

Bonan, G. B., 1994: Comparison of the land surface climatology of the National Center for Atmospheric Research Community Climate Model 2 at R15 and T42 resolutions. *J. Geophys. Res.,* **99,** 10 357–10 364.

Carlson, T. N., E. M. Perry, and T. J. Schmugge, 1990: Remote estimation of soil moisture availability and fractional vegetation cover over patchy vegetation. *Agric. Forest Meteor.,* **52,** 44–60.

Crosson, W. L., E. A. Smith, and H. J. Cooper, 1993: Estimation of surface heat and moisture fluxes over a prairie grassland. 4: Impact of satellite remote sensing of slow canopy variables on performance of a hybrid biosphere model. *J. Geophys. Res.,* **98,** 4979–4999.

Davis, R. E., 1976: Predictability of sea surface temperature and sea pressure anomalies over the North Pacific Ocean. *J. Phys. Oceanogr.,* **6,** 249–266.

Deardoff, J., 1978: Efficient prediction of ground surface temperature and moisture, with inclusion of a layer of vegetation. *J. Geophys. Res.,* **83,** 1153–1160.

Dickinson, R. E., 1989: Water and energy exchange. *Remote Sensing of Biosphere Functioning,* R. J. Hobbs and H. A. Mooney, Eds., Springer-Verlag, 105–133.

——, 1994: Satellite systems and models for future climate change. *World Survey of Climatology,* A. Henderson-Sellers, Ed., *Future Climates of the World,* Vol. 16.

——, and A. Henderson-Sellers, 1988: Modelling tropical deforestation: A study of GCM land-surface parameterizations. *Quart. J. Roy. Meteor. Soc.,* **114,** 373–388.

——, and P. J. Kennedy, 1991: Land surface hydrology in a general circulation model-global and regional fields needed for validation. *Surv. Geophys.,* **12,** 115–126.

——, ——, and M. F. Wilson, 1986: Biosphere–Atmosphere Transfer Scheme (BATS) for the NCAR Community Climate Model. NCAR Tech. Note NCAR/TN275+STR, 69 pp. [Available from National Center for Atmospheric Research, Boulder, CO 80307.]

——, ——, and ——, 1993: Biosphere–Atmosphere Transfer Scheme (BATS) Version 1E as Coupled to the NCAR Community Climate Model. NCAR Tech. Note NCAR/TN-387+STR, 72 pp. [Available from National Center for Atmosphere Research, Boulder, CO 80307.]

Garratt, J. R., 1995: Observed screen (air) and GCM surface/screen temperatures: Implications for outgoing longwave fluxes at the surface. *J. Climate,* **8,** 1360–1368.

Graddock, J. M., and C. R. Flood, 1969: Eigenvectors for representing the 500mb geopotential surface over the Northern Hemisphere. *Quart. J. Roy. Meteor. Soc.,* **95,** 576–593.

Hack, J. J., B. A. Boville, B. P. Briegleb, J. T. Kiehl, P. J. Rasch, and D. L. Williamson, 1993: Description of the NCAR Community Climate Model (CCM2). NCAR Tech. Note NCAR/TN-382-

STR, 108 pp. [Available from National Center for Atmospheric Research Boulder, CO 80307.]

——, ——, J. T. Kiehl, P. J. Rasch, and D. L. Williamson, 1994: Climate statistics from the National Center for Atmospheric Research community climate model CCM2. *J. Geophys. Res.*, **99,** 20 785–20 827.

Hahmann, A. N., D. M. Ward, and R. E. Dickinson, 1995: Land surface temperature and relative fluxes response of the NCAR CCM2/Biosphere–Atmosphere Transfer Scheme to modifications in the optical properties of clouds. *J. Geophys. Res.*, **100,** 23 239–23 252.

Hall, F. G., K. F. Huemmrich, S. J. Geotz, P. J. Sellers, and J. E. Nickeson, 1992: Satellite remote sensing of surface energy balance: Success, failures, and unsolved issues in FIFE. *J. Geophys. Res.*, **97,** 19 061–19 089.

Halpert, M. S., and C. F. Ropelewski, 1992: Surface temperature patterns associated with the Southern Oscillation. *J. Climate,* **5,** 577–593.

Haskins, R. D., T. P. Barnett, M. M. Tyree, and E. Roeckner, 1995: Comparison of cloud fields from AGCM, in situ and satellite measurements. *J. Geophys. Res.*, **100,** 1367–1387.

Henderson-Sellers, A., 1990: Predicting generalized ecosystem groups with the NCAR CCM: First step towards an interactive biosphere. *J. Climate,* **3,** 917–940.

——, M. F. Wilson, G. Thomas, and R. E. Dickinson, 1986: Current global land-surface data sets for use in climate-related studies. NCAR Tech. Note NCAR/TN272+STR, 110 pp. [Available from National Center for Atmospheric Research, Boulder, CO 80307.]

——, R. E. Dickinson, T. B. Durbidge, P. J. Kennedy, K. McGuffie, and A. J. Pitman, 1993: Tropical deforestation: Modeling local- to regional-scale climate change. *J. Geophys. Res.*, **98,** 7289–7315.

Hendon, H. H., and K. Woodberry, 1993: The diurnal cycle of the tropical convection. *J. Geophys. Res.*, **98,** 16 623–16 637.

Huband, N. D. S., and J. L. Monteith, 1986: Radiative surface temperature and energy balance of a wheat canopy. *Bound.-Layer Meteor.*, **36,** 1–17.

Jackson, T. J., D. M. Le Vine, A. J. Griffs, D. C. Goodich, T. J. Schmugge, C. T. Swift, and P. E. O'Neill, 1993: Soil moisture and rainfall estimation over a semiarid environment with ESTAR microwave radiometer. *IEEE Trans. Geosci. Remote Sen.,* **31,** 836–841.

Kidson, J. M., 1975: Tropical eigenvector analysis and the Southern Oscillation. *Mon. Wea. Rev.*, **103,** 187–196.

Kutzbach, J. E., 1970: Large-scale features of monthly mean Northern Hemisphere anomaly maps of sea-level pressure. *Mon. Wea. Rev.*, **98,** 708–716.

Matthew, E., 1983: Global vegetation and land use: New high-resolution data bases for climate studies. *J. Climate Appl. Meteor.*, **22,** 474–487.

——, 1984: Prescription of land-surface boundary conditions in GISS GCMII and vegetation, land-use and seasonal albedo data sets: Documentation of archived data tape. NASA Tech. Memos. 86096 and 86107, NASA/Goddard Institute for Space Studies, New York, NY, 20 pp and 9 pp.

Mintz, Y., and G. K. Walker, 1993: Global fields of soil moisture and land surface evapotranspiration derived from observed precipitation and surface air temperature. *J. Appl. Meteor.*, **32,** 1305–1334.

Nemani, R., L. Pierce, and S. Running, 1993: Developing satellite-derived estimates of surface moisture status. *J. Appl. Meteor.*, **32,** 548–557.

Olson, J. S., J. A. Watts, and L. J. Allison, 1983: Carbon in live vegetation of major world ecosystems. U.S. Dept of Energy DOE/NBB-0037 TR004, U.S. Dept. of Energy, Washington, DC, 152 pp.

Poetzsch-Heffter, C., Q. Liu, E. Ruprecht, and C. Simmer, 1995: Effect of cloud types on the Earth radiation budget calculated with the ISCCP C1 dataset: Methodology and initial results. *J. Climate,* **8,** 829–843.

Prata, A. J., V. Caselles, C. Coll, J. A. Sobrino, and C. Ottle, 1995: Thermal remote sensing of land surface temperature from satellites: Current status and future prospects. *Remote Sens. Rev.*, **12,** 124–175.

Sellers, P. J., S. I. Rasool, and H.-J. Bolle, 1990: A review of satellite data algorithms for studies of the land surface. *Bull. Amer. Meteor. Soc.*, **71,** 1429–1447.

——, F. G. Hall, G. Asrar, D. E. Strebel, and R. E. Murphy, 1992: An overview of the First International Satellite Land Surface Climatology Project (ISLSCP) Field Experiment (FIFE). *J. Geophys. Res.*, **97,** 18 345–18 371.

Smith, E. A., H. J. Cooper, W. L. Crosson, and W. Heng-Yi, 1993: Estimation of surface heat and moisture fluxes over a prairie grassland. 3: Design of a hybrid physical/remote sensing biosphere model. *J. Geophys. Res.*, **98,** 4951–4978.

Smith, W. L., H. M. Woolf, and C. M. Hayden, 1979: The TIROS-N Operational Vertical Sounder. *Bull. Amer. Meteor. Soc.*, **60,** 1177–1187.

Soden, B. J., and F. P. Bretherton, 1994: Evaluation of water vapor distribution in general circulation models using satellite observations. *J. Geophys. Res.*, **99,** 1187–1210.

Sun, J., and L. Mahart, 1995: Determination of surface fluxes from the surface radiation temperature. *J. Atmos. Sci.*, **52,** 1096–1106.

Susskind, J., 1993: Water vapor and temperature. *Atlas of Satellite Observations Related Global Change,* R. J. Gurney, J. L. Foster, and C. L. Parkinson, Eds., Cambridge University Press, 89–128.

——, D. Rosenfield, and M. T. Chahine, 1984: Remote sensing of weather and climate parameters from HIRS2/MSU on TIROS-N. *J. Geophys. Res.*, **89,** 4677–4697.

Tran, A. V., E. Smith, J. Hyon, R. Evans, O. Brown, and G. Feldman, 1992: Satellite-Derived Multichannel Sea-Surface Temperature and Phytoplankton Pigment Concentration Data: A CD-ROM Set Containing Monthly Mean Distributions for the Global Oceans. Jet Propulsion Laboratory, JPL D-1035-1.

Trenberth, K. E., and D. A. Paolino Jr., 1981: Characteristic patterns of variability of sea level pressure in the Northern Hemisphere. *Mon. Wea. Rev.*, **109,** 1169–1189.

Tselioudis, G., W. B. Rossow, and D. Rind, 1992: Global patterns of cloud optical thickness variation with temperature. *J. Climate Appl. Meteor.*, **5,** 1484–1495.

van Loon, H., and J. C. Rogers, 1978: The seesaw in winter temperatures between Greenland and Northern Europe. Part I: General description. *Mon. Wea. Rev.*, **106,** 296–310.

Vining, R. C., and B. L. Blas, 1992: Estimation of sensible heat flux from remotely sensed canopy temperature. *J. Geophys. Res.*, **97,** 18 951–18 954.

Walker, G. T., and E. W. Bliss, 1932: World Weather V. *Mem. Roy. Meteor. Soc.*, **4,** 53–84.

Wallace, J. M., and D. S. Gutzler, 1981: Teleconnections in the geopotential height field during the Northern Hemisphere winter. *Mon. Wea. Rev.*, **109,** 784–812.

Wang, J. R., 1992: Active and passive microwave measurements of soil moisture in FIFE. *J. Geophys. Res.*, **97,** 18 979–18 985.

Wetzel, P. J., and R. H. Woodward, 1987: Soil moisture estimation using GOES-VISSR infrared data: A case study with a simple statistical method. *J. Climate Appl. Meteor.*, **26,** 107–117.

Wilson, M. F., A. Henderson-Sellers, R. E. Dickinson, and P. J. Kennedy, 1987a: Sensitivity of the Biosphere–Atmosphere Transfer Scheme (BATS) to the inclusion of variable soil characteristics. *J. Appl. Meteor.*, **26,** 341–362.

——, ——, ——, and ——, 1987b: Investigation of the sensitivity of the land-surface parameterization of the NCAR Community Climate Model in region of tundra vegetation. *J. Climate,* **7,** 319–343.